

Full Proximity Treatment of Topological Superconductors in Josephson Junction Architectures

F. Setiawan,^{1,*} Chien-Te Wu,^{2,1} and K. Levin¹

¹*James Franck Institute, University of Chicago, Chicago, Illinois 60637, USA*

²*Department of Electrophysics, National Chiao Tung University, Hsinchu, Taiwan*

Experiments on planar Josephson junction architectures have recently been shown to provide an alternative way of creating topological superconductors hosting accessible Majorana modes. These zero-energy modes can be found at the ends of a one-dimensional channel in the junction of a two-dimensional electron gas (2DEG) proximitized by two spatially separated superconductors. The channel, which is below the break between the superconductors, is not in direct contact with the superconducting leads, so that proximity coupling is expected to be weaker and less well-controlled than in the simple nanowire configuration widely discussed in the literature. This provides a strong incentive for this paper which investigates the nature of proximitization in these Josephson architectures. At a microscopic level we demonstrate how and when it can lead to topological phases. We do so by going beyond simple tunneling models through solving self-consistently the Bogoliubov-de Gennes equations of a heterostructure multicomponent system involving two spatially separated *s*-wave superconductors in contact with a normal Rashba spin-orbit-coupled 2DEG. Importantly, within our self-consistent theory we present ways of maximizing the proximity-induced superconducting gap by studying the effect of the Rashba spin-orbit coupling and chemical potential mismatch between the superconductor and 2DEG, and sample geometry on the gap. Finally, we note (as in experiment) a Fulde-Ferrell-Larkin-Ovchinnikov phase is also found to appear in the 2DEG channel, albeit under circumstances which are not ideal for topological superconducting phase.

I. INTRODUCTION

There has been much excitement in the literature over the possibility of observing one-dimensional (1D) topological superconductivity which involves a single 1D wire [1, 2] leading to accessible Majorana zero modes. Because of fluctuation effects in low dimensions, there can be no intrinsic superconductivity so that the focus is on proximitized superconductors. Studies of these wires and their applications towards quantum computation have led to a very extensive literature [3–10]. In a broad sense, there are two general configurations for proximitized 1D topological superconductors. These are associated with “nanowires” in direct contact with superconducting hosts as well as the recently proposed planar Josephson junction [11, 12]. The latter contains a proximitized 1D channel in the two-dimensional electron gas (2DEG) just below the break between the two superconductors. This configuration is less widely studied, but there is evidence, as in the simple nanowires [13–33], that topological superconductivity has been experimentally observed [34, 35].

Indeed, the planar junctions have a notable strength relative to the nanowires. The phase difference between the two superconductors provides an alternative knob (beyond the Zeeman field) to tune the system into the topological phase [11, 12]. In ideal (i.e., transparent) systems, when the superconducting phase difference is $\phi = \pi$, the topological phase can be achieved for rather small Zeeman fields. However, compared to the prox-

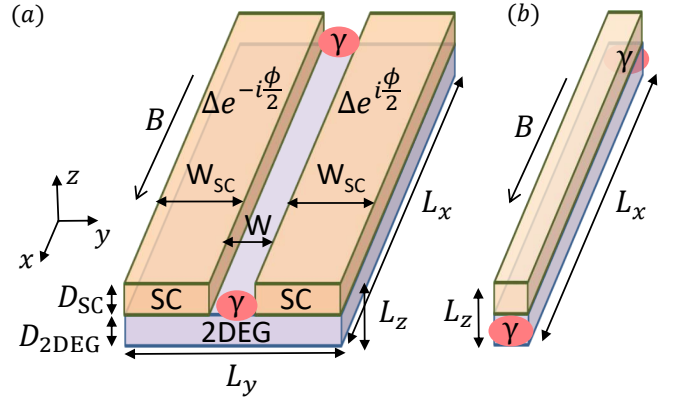


FIG. 1. (a) Schematic diagram of a 2DEG in proximity with two spatially separated superconducting leads which form a Josephson junction. By tuning the strength of either the applied in-plane magnetic field B or the phase difference ϕ between the two superconductors, the system can be tuned into the topological superconducting phase which hosts Majorana zero modes (γ) at the end of the junction. (b) Schematic diagram of a nanowire proximitized by a superconductor. The system becomes a topological superconductor, which hosts Majorana zero modes (γ) at the end of the nanowire, when the strength of the magnetic field B is above a certain critical value.

imitized nanowire, the planar Josephson junction architecture is associated with weaker and less well-controlled proximitization, as the 1D channel in the junction is not in direct contact with the host superconductors.

This leads to the central goal of this paper which is to quantify this somewhat indirect form of proximitization and to optimize its effectiveness. We focus on a

* setiawan@uchicago.edu

well-studied substrate: the 2DEG which has moderately strong Rashba spin-orbit coupling (SOC). Our calculations go beyond the simple tunneling models [36–40] of the proximity effect by solving the full Bogoliubov-de Gennes (BdG) equations of a multicomponent system with self consistency. (Although not all of the results presented in this paper are fully self-consistent, we have checked a few cases that increasing the number of iterations only very slightly modifies our results.) In our full proximity model, the host superconductors are treated as a participating component rather than as a passive source of Cooper pairing. The effectiveness of proximitization is quantified via the strength of the induced pairing amplitude, Δ^{prox} . Maximizing this pairing amplitude is the goal as it is associated with a large gap in the dispersion. This, in turn, leads to more localized and thus more stable Majorana modes. In this paper we characterize the deleterious effects on Δ^{prox} which can come from any of the following: SOC, enhanced substrate thickness, enhanced channel width, and chemical potential differences (between the host superconductors and the 2DEG). Importantly, our findings which are obtained using a fully self-consistent theory, can provide guidance in determining the optimal range of experimental parameters for the topological protection of Majorana modes.

While not essential to the topological superconductivity, a relevant complement to these studies relates to a very elusive state of matter, the Fulde-Ferrell-Larkin-Ovchinnikov (FFLO) [41, 42] phase which we also observe in these planar junctions. This appears to be consistent with recent experiments which have reported that this otherwise rare phase of superconductivity is realized in proximitized superconductors [43, 44]. For the situation here, it can be viewed as arising from a “second-order proximitization” process. We trace its origin to the fact that the channel makes little direct contact with the superconductors, unlike the rest of the proximitized 2DEG. Thus, in this region of the junction, the pairing amplitude is reduced and the effective small pairing gap is freer to oscillate in response to an applied Zeeman field. We finally note that this FFLO phase is most apparent in relatively wide junctions where the gap is smaller and it is thus unfavorable for stabilizing a topological phase.

The two generic types of proximitized 1D topological superconductors are illustrated in Fig. 1. The Majorana zero-modes (indicated by γ) appear at the ends of the junction where they are most easily manipulated. In structures as shown in Fig. 1(a), the substrate is usually a Rashba spin-orbit-coupled 2DEG. Figure 1(b) shows a more successful variant of these hybrid structures which involve semiconducting nanowires (although chains of magnetic atoms [45–51] and topological insulators [52–54] have also been considered).

One should appreciate that were one to design topological quasi-1D superconductors [55] without proximitization, say by doping a topological insulator, there is less control in engineering the appropriate combination of SOC, Zeeman field and band structure in the presence

of sufficiently strong pairing attraction. The existence of these intrinsic topological superconductors is still controversial so that, currently, proximity-induced superconductivity appears to be an essential tool. And because it is so essential it is imperative to understand it better, not just in the immediate interface, which has been studied [38–40], but well into the depth of a hypothesized topological superconductor [56, 57].

A. Overview and Outline

It is useful to quantitatively characterize the Josephson-based topological superconductors we consider here in terms of the size of the energy gap, E_{gap} , associated with the proximitized 2DEG. The quantity E_{gap} depends on the junction geometry and materials parameters. It varies with the junction thickness, the strip width, the SOC and chemical potential difference between the host superconductors and the 2DEG. Equally important is its dependence on the external parameters which control topological phases: the Josephson junction phase difference ϕ and the Zeeman field E_Z . This field enters in two different ways; it affects the gap opening and closing processes associated with topological phase transitions in a Josephson junction. It also affects the coupling at each separate interface between the host superconductor and the 2DEG substrate. Increasing E_Z in the 2DEG inhibits proximitization.

It is convenient, then, to isolate these processes by writing

$$E_{\text{gap}} \equiv \Delta^{\text{prox}}|_{(E_Z=\phi=0)} f(E_Z, \phi). \quad (1)$$

This states that the energy gap in the presence of Zeeman and superconducting phase difference, E_{gap} depends directly on a proximity-induced gap Δ^{prox} , (which is deduced in the absence of any Zeeman field, E_Z or phase bias ϕ) times a multiplicative function, $f(E_Z, \phi)$, which represents (dominantly) the topological characteristics of the junction.

In the topological region, the parameter E_{gap} is, thus, a crucial parameter, as its inverse characterizes the Majorana localization length. The smaller this length, the more localized are the Majorana modes. The localization of the Majoranas is, then, optimized when the proximity gap Δ^{prox} is maximal. Understanding this is one of the central contributions of our paper.

We now present a brief outline. Section II of the paper discusses the theoretical model, i.e., the Hamiltonian of the planar Josephson junction. In Sec III, we give a discussion of the self-consistent BdG approach used to solve for the energy dispersion and proximity-induced gap. In Sec. IV we study a simple tunneling model of the superconducting proximity effect in which the junction is converted to a lower dimension by integrating out the host superconductors. Section V focuses on numerical results from our full-proximity model for the proximity gap

Δ^{prox} where Δ^{prox} is the spectral gap calculated for junctions in the absence of Zeeman field and superconducting phase difference. Here we separately discuss the role of SOC, chemical potential mismatch and 2DEG thickness on Δ^{prox} . The symmetry class of the planar Josephson junction is addressed in Sec. VI. In Sec. VII we present the topological phase diagram as a function of in-plane Zeeman field and superconducting phase bias. We further show the evolution of the energy spectrum across the topological phase transition. Sec. VIII presents a brief discussion of how FFLO superconducting phase is established, where, again, the Zeeman field is present. More details of this elusive FFLO phase are presented in an appendix A. Finally, we summarize our conclusions in Sec. IX.

II. THEORETICAL MODEL

We consider a Josephson junction made from a Rashba spin-orbit-coupled 2DEG in contact with two spatially separated superconductors and subjected to an in-plane magnetic field along the junction as shown in Fig. 1(a). This system was proposed recently [11, 12] as a new platform to realize topological superconductors. In this setup, the transition between the trivial and topological phases can be tuned by varying either the applied in-plane magnetic field B along the junction or the phase difference ϕ between the two superconductors. In an ideal situation, the interplay between these two independent knobs enables a lower critical field for the topological transition to be achieved when the superconducting phase difference is tuned near $\phi = \pi$. This Zeeman- and phase-tunable topological transition was demonstrated in recent experiments [34, 35].

A. Hamiltonian

We begin by writing down the “normal” component (in the absence of superconducting pairing) of the Hamiltonian as

$$H = \int d^3\mathbf{r} \sum_{\sigma\sigma'} \psi_{\sigma}^{\dagger}(\mathbf{r}) \left[\left(\frac{\mathbf{P}^2}{2m^*} - \mu(\mathbf{r}) \right) \sigma_0 + E_Z(\mathbf{r}) \sigma_x + \alpha(\mathbf{r}) (P_x \sigma_y - P_y \sigma_x) \right] \psi_{\sigma'}(\mathbf{r}), \quad (2)$$

where ψ_{σ} (ψ_{σ}^{\dagger}) is the annihilation (creation) operator of an electron with spin $\sigma = \uparrow, \downarrow$. In Eq. (2), σ_0 is the identity matrix and $\boldsymbol{\sigma} \equiv (\sigma_x, \sigma_y, \sigma_z)$ are the Pauli matrices acting on the spin degree of freedom. Here, \mathbf{P} represents the real space momentum operator, m^* is the effective electron mass, μ is the chemical potential. The Zeeman energy $E_Z(\mathbf{r}) = \tilde{g}(\mathbf{r}) \mu_B B/2$ is due to the applied in-plane magnetic field B along the junction (x direction) with \tilde{g} being the Lande g -factor and μ_B being the Bohr magneton. An important parameter which appears throughout

this paper is α which characterizes the strength of the SOC in the 2DEG. The SOC strength is zero in the superconductors and insulator but finite in the 2DEG, i.e.,

$$\alpha(\mathbf{r}) = \begin{cases} 0 & \text{for } D_{2\text{DEG}} < z < D_{2\text{DEG}} + D_{\text{SC}}, \\ \alpha & \text{for } 0 < z < D_{2\text{DEG}}, \end{cases} \quad (3)$$

where D_{SC} and $D_{2\text{DEG}}$ denote the thicknesses of the superconductors and the 2DEG, respectively [Fig. 1(a)]. This is a realistic representation [58, 59] of the well-studied situation of a spin-orbit-coupled semiconductor proximitized by an s -wave superconductor.

The chemical potentials are taken to be

$$\mu(\mathbf{r}) = \begin{cases} \mu_S & \text{for } W/2 < |y| < W_{\text{SC}} + W/2 \\ & \text{and } D_{2\text{DEG}} < z < D_{2\text{DEG}} + D_{\text{SC}}, \\ \mu_I & \text{for } 0 < |y| < W/2 \\ & \text{and } D_{2\text{DEG}} < z < D_{2\text{DEG}} + D_{\text{SC}}, \\ \mu_{2\text{DEG}} & \text{for } |y| < W_{\text{SC}} + W/2 \\ & \text{and } 0 < z < D_{2\text{DEG}}, \end{cases} \quad (4)$$

where μ_S , μ_I and $\mu_{2\text{DEG}}$ are the chemical potentials of the superconductor, insulator and 2DEG, respectively. The widths of the superconductors and the junction (along y direction) are denoted by W_{SC} and W , respectively. In this paper we consider the width of the superconducting leads $W_{\text{SC}} > \xi$ where ξ is the superconducting coherence length. Throughout this paper, we work in units where $\hbar = 1$, $\mu_{2\text{DEG}} = 1$, and $2m^* = 1$ which gives the Fermi momentum of the 2DEG, $k_F = 1$. Note that for numerical simplicity, we introduce an insulator in between the superconductors. Its chemical potential is taken to be very negative ($\mu_I = -5$), so that it behaves essentially as a vacuum. Except when indicated otherwise, the Zeeman energy $E_Z(\mathbf{r})$ is assumed to be zero in the host superconductor and insulator but taken to be constant throughout the 2DEG ($E_{Z,L} = E_{Z,J} = E_Z$, where $E_{Z,L}$ is the Zeeman energy of the 2DEG directly below the superconducting leads and $E_{Z,J}$ is the Zeeman energy of the 2DEG in the junction).

So far we have described a non-interacting system. Now, let us include the superconducting pairing term in the Hamiltonian, which is given by

$$\sum_{\sigma\sigma'} (i\sigma_y)_{\sigma\sigma'} \Delta(\mathbf{r}) \psi_{\sigma}^{\dagger}(\mathbf{r}) \psi_{\sigma'}^{\dagger}(\mathbf{r}) + \text{H.c.} \quad (5)$$

We assume that the system is translationally invariant along the \hat{x} direction and finite in both \hat{y} and \hat{z} directions. Because the system is translationally invariant along the x direction, we can write the Hamiltonian in the Nambu basis $\Psi_{k_x}(y, z) = [\psi_{k_x\uparrow}(y, z), \psi_{k_x\downarrow}(y, z), \psi_{k_x\downarrow}^{\dagger}(y, z), -\psi_{k_x\uparrow}^{\dagger}(y, z)]^T$ as

$$H = \frac{1}{2} \int dk_x \int dz \int dy \Psi_{k_x}^{\dagger}(y, z) \mathcal{H}_{k_x}(y, z) \Psi_{k_x}(y, z), \quad (6)$$

where the BdG Hamiltonian is given by

$$\begin{aligned}\mathcal{H}_{k_x}(y, z) = & [k_x^2 - \partial_y^2 - \partial_z^2 - \mu(y, z)] \tau_z \\ & + \alpha(z)(k_x \sigma_y + i \partial_y \sigma_x) \tau_z + E_Z(y, z) \sigma_x \\ & + \Delta(y, z) \tau_+ + \Delta^*(y, z) \tau_-, \end{aligned} \quad (7)$$

Here the Pauli matrices σ and τ act in the spin and particle-hole subspace, respectively, with $\tau_{\pm} = (\tau_x \pm i \tau_y)/2$. The superconducting pairing potential, $\Delta(y, z)$, arises microscopically from the attractive interactions which are only present in the host superconductors:

$$\Delta(y, z) \equiv g(y, z) F(y, z), \quad (8)$$

where $g(y, z)$ is the coupling function within the host:

$$g(y, z) = \begin{cases} g_0 e^{-i\phi/2} & \text{for } -(W_{\text{SC}} + W/2) < y < -W/2 \\ & \text{and } D_{2\text{DEG}} < z < D_{2\text{DEG}} + D_{\text{SC}}, \\ g_0 e^{i\phi/2} & \text{for } W/2 < y < W_{\text{SC}} + W/2 \\ & \text{and } D_{2\text{DEG}} < z < D_{2\text{DEG}} + D_{\text{SC}}, \\ 0 & \text{otherwise.} \end{cases} \quad (9)$$

Here, g_0 is the attractive coupling constant, ϕ is the phase difference between the two superconductors. Applying a Bogoliubov transformation, $\psi_{k_x \sigma} = \sum_n [u_{nk_x \sigma} \gamma_n + v_{nk_x \sigma}^* \gamma_n^\dagger]$ [60, 61], we then obtain the pair amplitude

$$\begin{aligned} F(y, z) &= \langle \psi_\uparrow(y, z) \psi_\downarrow(y, z) \rangle \\ &= \int dk_x \sum_{E_n < \omega_D} [u_{nk_x \uparrow} v_{nk_x \downarrow}^* - u_{nk_x \downarrow} v_{nk_x \uparrow}^*] \\ &\quad \times \tanh\left(\frac{E_n}{2T}\right), \end{aligned} \quad (10)$$

where T is the temperature. The Debye frequency ω_D provides an energy cutoff in Eq. (10). Note that, through the proximity effect, the pair amplitude $F(y, z)$ in the 2DEG is non-zero even though there is a vanishing order parameter, $\Delta = 0$, reflecting the fact that $g(y, z) = 0$ there. The superconducting pairing potential $\Delta(y, z)$ is obtained by solving the BdG Hamiltonian self-consistently as explained in the next subsection.

III. SELF-CONSISTENT BdG EQUATION

We obtain the pair amplitude $F(y, z)$ [Eq. (10)] by numerically solving the BdG eigenvalue problem following the scheme developed in Refs. [60–63]. The scheme is based on the idea of recasting the original Hamiltonian, Eq. (6) in the basis that diagonalizes the Hamiltonian. By numerically diagonalizing, we solve for the wave function of the BdG equations:

$$\mathcal{H}_{k_x}(y, z) \Phi_{nk_x}(y, z) = E_n \Phi_{nk_x}(y, z) \quad (11)$$

where the wave function is given by

$$\Phi_{nk_x}(y, z) = \begin{pmatrix} u_{nk_x \uparrow}(y, z) \\ u_{nk_x \downarrow}(y, z) \\ v_{nk_x \downarrow}(y, z) \\ -v_{nk_x \uparrow}(y, z) \end{pmatrix}, \quad (12)$$

with the boundary condition $\Phi_{nk_x}(y, z) = 0$ at $|y| > W_{\text{SC}} + W/2$, $z < 0$ and $z > D_{2\text{DEG}} + D_{\text{SC}}$ and subject to the self-consistency equation [Eqs. (8)–(10)]. To this end, we expand both the matrix elements and the eigenfunctions in terms of a Fourier basis. Specifically, the quasi-particle ($u_{nk_x \sigma}$) and quasi-hole ($v_{nk_x \sigma}$) wavefunctions are given by

$$u_{nk_x \sigma}(y, z) = \frac{2}{\sqrt{L_y L_z}} \sum_{pq} u_{nk_x \sigma}^{pq} \sin\left(\frac{p\pi y}{L_y}\right) \sin\left(\frac{q\pi z}{L_z}\right), \quad (13a)$$

$$v_{nk_x \sigma}(y, z) = \frac{2}{\sqrt{L_y L_z}} \sum_{pq} v_{nk_x \sigma}^{pq} \sin\left(\frac{p\pi y}{L_y}\right) \sin\left(\frac{q\pi z}{L_z}\right). \quad (13b)$$

For definiteness, we set the smallest length scale to be of the order of $1/k_F$ where $k_F = \sqrt{\mu_{2\text{DEG}}}$ is the Fermi momentum of the 2DEG.

General matrix elements are similarly expanded in terms of the same Fourier series. For example, we define the matrix elements of an operator O to be

$$\begin{aligned} O^{pq p' q'} &\equiv \langle pq | O | p' q' \rangle \\ &= \frac{4}{L_y L_z} \int_0^{L_y} \int_0^{L_z} dy dz \sin\left(\frac{p\pi y}{L_y}\right) \sin\left(\frac{q\pi z}{L_z}\right) \\ &\quad \times O \sin\left(\frac{p'\pi y}{L_y}\right) \sin\left(\frac{q'\pi z}{L_z}\right). \end{aligned} \quad (14)$$

In this way all terms in the BdG Hamiltonian can be expanded in this basis set. What we have accomplished in this procedure is to successfully transform a set of differential equations into an algebraic matrix eigenvalue problem.

Having recast the Hamiltonian in the basis given in Eq. (13), we then solve for the pair amplitude using Eqs. (8)–(10) from the wavefunction obtained by diagonalizing the Hamiltonian. The calculated pair amplitude is then used to get a new wavefunction [Eq. (11)]. This self-consistent procedure is carried out repeatedly until convergence is reached. The first iteration generally contains the central physics. Because of the numerical complexity of the full-proximity model and the many parameter sets we address, in many plots we restrict ourselves to the first iteration; in a few such cases we have confirmed that higher iterations introduce changes in the solution of only a few percent. Throughout this paper, the pair amplitude $F(y, z)$ is calculated by setting the parent superconductor pair potential, $\Delta_0 = 0.3$, Debye frequency $\omega_D = 0.5$ and temperature $T = 0$ in Eq. (10).

IV. TUNNELING APPROXIMATION TO PROXIMITIZATION

The above, more powerful procedure has not been widely applied; rather the literature focus has been on an approximate treatment of proximitization. The approximate approach builds on earlier work by McMillan [36, 37], who introduced a perturbative treatment of a tunneling Hamiltonian for a single NS junction which consists of a normal metal in proximity to a superconductor. This treatment was later extended by Refs. [38–40] to deal with a spin-orbit-coupled electron gas or a topological insulator in proximity with a superconductor. In this section we use N and S to represent the 2DEG and superconductor, respectively; both are considered to be sufficiently thin so that any spatial variations within each can be ignored. The Hamiltonian for the SC/2DEG heterostructure can be written as

$$H = H_S + H_N + H_T. \quad (15)$$

Here, $H_{S,N}$ is the Hamiltonian of the superconductor (S) and 2DEG (N), respectively and the tunneling Hamiltonian is given by

$$H_T = \sum_{SN} t(c_{S,k,\uparrow}^\dagger c_{N,k',\uparrow} + c_{S,k,\downarrow}^\dagger c_{N,k',\downarrow}) + \text{h.c.}, \quad (16)$$

where $c_{S/N,k,\sigma}$ is the annihilation operator in the S or N side of the interface for an electron with momentum k and spin $\sigma = \uparrow/\downarrow$. The tunnel coupling t couples the sites of the superconductor and 2DEG which are directly next to each other on the NS interface.

In this approach one derives the proximity-induced superconductivity by integrating out the superconducting term in Eq. (15) and calculating the surface self-energy due to the electron tunneling between the 2DEG and superconductor.

Assuming that the density of states to be weakly dependent on energy, the surface self-energy can be calculated to be [38, 64]

$$\begin{aligned} \Sigma_N(\omega) &= |t|^2 \nu(\varepsilon_{F_N}) \int d\varepsilon G_S(\varepsilon, \omega) \\ &= -|t|^2 \nu(\varepsilon_{F_N}) \left[\frac{\omega \tau_0 + \Delta_0 \tau_x}{\sqrt{\Delta_S^2 - \omega^2}} + \zeta \tau_z \right], \end{aligned} \quad (17)$$

where the density of states $\nu(\varepsilon_{F_N})$ is evaluated at the Fermi energy of the 2DEG and ζ is the proximity-induced shift in the chemical potential. We can now incorporate this self-energy into the Green's function of the 2DEG, where we have

$$G_N(\mathbf{k}, \omega) = \frac{Z_{\Gamma_N}}{\omega - Z_{\Gamma_N} H_N - (1 - Z_{\Gamma_N}) \Delta_S \tau_x}. \quad (18)$$

Here

$$Z_{\Gamma_N}(\omega) = \left(1 + \frac{\Gamma_N}{\sqrt{\Delta_S^2 - \omega^2}} \right)^{-1} \quad (19)$$

is the reduced quasiparticle weight due to the virtual propagation of electrons in the superconductor with $\Gamma_N = |t|^2 \nu(\varepsilon_{F,N})$ being the effective coupling between the 2DEG and superconductor. Equivalent equations can be written for the self-energy of the superconductor $\Sigma_S(\omega)$, by just exchanging N for S in the above expressions. This gives coupled gap equations:

$$\Delta_N = (1 - Z_{\Gamma_N}) \Delta_S, \quad (20a)$$

$$\Delta_S = Z_{\Gamma_S} \Delta_0 + (1 - Z_{\Gamma_S}) \Delta_N, \quad (20b)$$

where $\Delta_{N,S}$ is the renormalized superconducting pairing potential in the 2DEG (N) and superconductor (S), respectively, and Δ_0 is the gap in the isolated superconductor. The above coupled gap equations reflect the fact that proximitization is a two-way process. It introduces a pairing gap in a normal material and at the same time it renormalizes the excitation gap in the host superconductor.

A. Relation to the standard effective model

In the literature it is rather common to ignore the corrections in the host superconductor and assume $\Delta_S = \Delta_0$ but we will see in the full proximitization theory that this is not generally the case. Also important is that in the more general situation, all pair amplitude parameters vary continuously across the system.

With this simplification, the above analysis is the basis for the so-called “effective model” which is described as having integrated out the host superconductor. In the effective model, the Hamiltonian of the 2DEG is given by [11, 12]

$$\begin{aligned} \mathcal{H}_{k_x} &= (k_x^2 - \partial_y^2 - \partial_z^2 - \mu) \tau_z + \alpha(k_x \sigma_y + i \partial_y \sigma_x) \tau_z \\ &\quad + E_Z(y) \sigma_x + \Delta(y) \tau_+ + \Delta^*(y) \tau_-, \end{aligned} \quad (21)$$

where Δ is the proximity-induced pairing potential in the 2DEG which is obtained after integrating out the superconductors. This is given by

$$\Delta(y) = \begin{cases} \Delta^{\text{prox}} e^{-i\phi/2} & \text{for } -(W_{\text{SC}} + W/2) < y < -W/2, \\ 0 & \text{for } -W/2 < y < W/2, \\ \Delta^{\text{prox}} e^{i\phi/2} & \text{for } W/2 < y < W_{\text{SC}} + W/2, \end{cases} \quad (22)$$

where Δ^{prox} is chosen phenomenologically.

V. UNDERSTANDING THE PROXIMITY-INDUCED GAP Δ^{prox}

We turn now to numerical results for Δ^{prox} obtained from our full proximitization studies. Although we begin with the limit of zero magnetic field, it is useful, to understand how the magnetic field affects the separate proximitization processes at each of the two interfaces

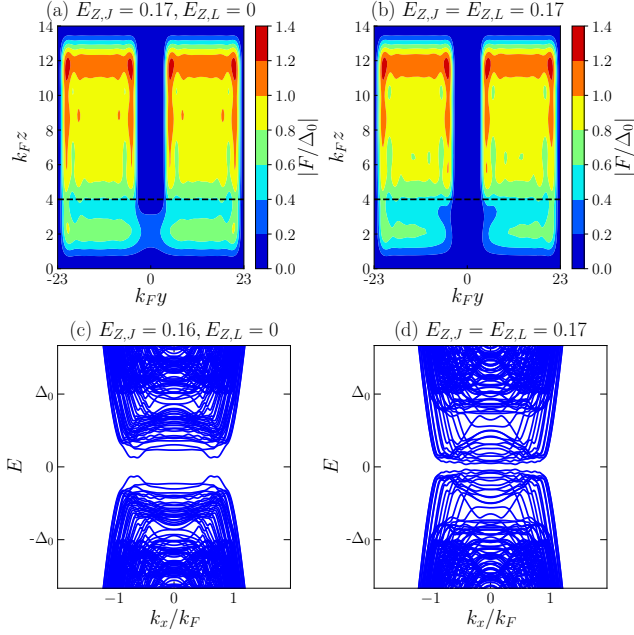


FIG. 2. Profile of pair amplitudes (Top panel) and energy spectra (Bottom panel) of the planar Josephson junction for the case: (Left panel) Zeeman is only in the junction ($E_{Z,J} = 0.17$ and $E_{Z,L} = 0$) and (Right panel) Zeeman is uniform across the 2DEG ($E_{Z,J} = E_{Z,L} = 0.17$). Note that the presence of the Zeeman field in the 2DEG below the superconductor ($E_{Z,L}$) reduces the induced pair amplitude and proximity gap in the 2DEG [panel (b) and (d)]. The black dashed lines in top panel denote the boundaries between the superconductors and the 2DEG. The parameters used are $\mu_S = 1$, $\mu_{2DEG} = 1$, $\alpha = 0.05$, $\Delta_0 = 0.3$ [$\xi = v_F/(\pi\Delta_0) = 2.12$], $\phi = 0$, $W_{SC} = 20/k_F$, $W = 6/k_F$, $D_{SC} = 10/k_F$ and $D_{2DEG} = 4/k_F$.

between the 2DEG and the host superconductor. To do this we compare two kinds of Josephson junction configuration: the first junction has the Zeeman field confined to the channel in the 2DEG between the two superconductors [Figs. 2(a) and 2(c)] and the second junction has the field applied uniformly in the 2DEG substrate [Figs. 2(b) and 2(d)], as in experiments.

The upper panels in Fig. 2 present contour plots of the pair amplitudes and the lower plots show the energy dispersions. One can see that a magnetic field below the superconductors has very little effect back on the parent superconductors but, as expected, it does decrease the pair amplitude and energy gap in the 2DEG. Fortunately with the planar Josephson junction design, we can tune the phase difference towards π such that the critical field for the transition into the topological phase is smaller such that there is still a substantial gap present when the system is in the topological phase.

In the remainder of this section, we will address how to optimize the proximity gap Δ^{prox} at $E_Z = \phi = 0$. By dropping the Zeeman field and junction phase bias, we are establishing how to select materials as well as geometric parameters.

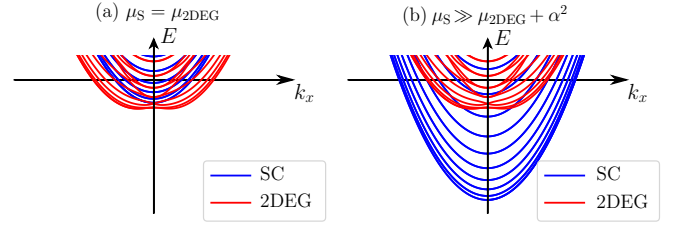


FIG. 3. Understanding effects of chemical potential mismatch on proximitization. Energy spectra of the normal part of the Hamiltonian of the superconductor (SC) and 2DEG for the case where (a) $\mu_S = \mu_{2DEG}$ and (b) $\mu_S \gg \mu_{2DEG} + \alpha^2$. For the case where (a) $\mu_S = \mu_{2DEG}$, the mismatch between the Fermi momenta of the SC and 2DEG gets larger for increasing SOC strength α while for the case where (b) $\mu_S \gg \mu_{2DEG} + \alpha^2$, the mismatch between the Fermi momenta of the SC and 2DEG is weakly dependent on the SOC strength α . In summary, the dependence of the proximity gap Δ^{prox} on α is weaker for the case where the SC chemical potential is much larger than the 2DEG chemical potential.

A. Effects of variable spin-orbit coupling and chemical potential mismatch

Since SOC plays an important role, it should be noted that there is no consensus in the literature about how SOC interacts with proximitization. It has been argued that larger SOC is beneficial [40]. We find here, that in the absence of a magnetic field, the effects of SOC on the proximity-induced gap are strongly tied to size of the chemical potential difference between the superconductors and the 2DEG. This can be understood in large part because of a mismatch in the Fermi momenta of the bands in the superconductors with that of the spin-orbit-coupled 2DEG.

This mismatch is illustrated in Fig. 3. Here the left panel (a) shows the superposed normal-state dispersions for the case where the superconductor and spin-orbit-coupled 2DEG have the same chemical potential and the right panel (b) is for the case where the chemical potential in the superconductor is much larger than that in the 2DEG, as is more often the case. The principal conclusion from panel (a) is that there are many bands in 2DEG which have little Fermi momentum overlap (because of the shift due to SOC in the 2DEG) with bands in the superconductors; one can anticipate that this mismatch increases as SOC becomes larger. This is in contrast to panel (b) where all bands in the 2DEG have their Fermi momenta close to those in the superconductor. Here the deleterious effects of SOC on the proximity-induced gap will be less apparent.

We summarize this by noting that the dependence of the proximitized gap on the SOC strength is weaker for the case where the superconductor chemical potential is larger than the 2DEG chemical potential. This is because a superconductor with a larger chemical potential has more occupied subbands. As a result, for an incident electron coming from the 2DEG with transverse momen-

tum normal to the NS interface, there is an electron from one of the subbands in the superconductor with momentum which is close to matching the incident momentum of the electron from the 2DEG.

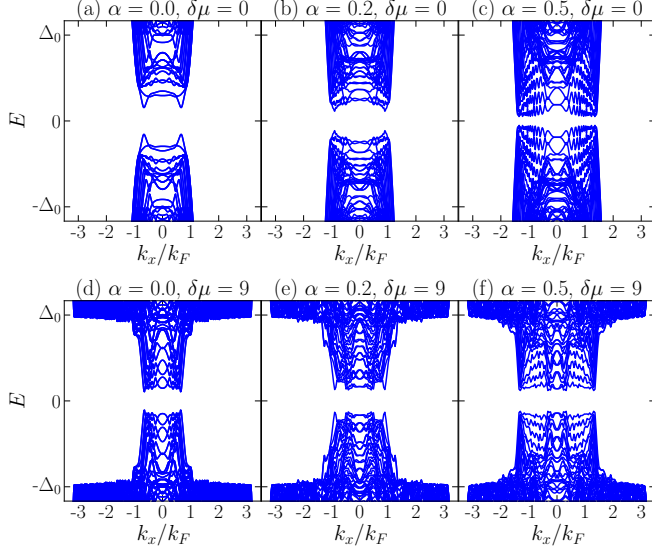


FIG. 4. Effects of SOC on the spectral gap for the case where there is no magnetic field. Top panel: For small chemical potential mismatch, e.g., $\delta\mu = \mu_S - \mu_{2\text{DEG}} = 0$, the gap depends strongly on the 2DEG SOC. The gap decreases with increasing SOC strength as shown in panels (a)-(c) because there is a larger mismatch between the Fermi momentum of the superconductor and Rashba spin-orbit-coupled 2DEG as the SOC strength increases. Bottom panel: For large chemical potential mismatch, e.g., $\delta\mu = \mu_S - \mu_{2\text{DEG}} = 9$, the gap depends weakly on the 2DEG SOC [see panels (d)-(f)] as there are more occupied subbands in superconductors with large μ_S . This implies that for an incident electron coming from the one of the band of the 2DEG, there is a band in the superconductor with a momentum close to the incident momentum. The parameters used are $\mu_{2\text{DEG}} = 1$, $E_{Z,J} = E_{Z,L} = 0$, $\Delta_0 = 0.3$, $\phi = 0$, $W_{\text{SC}} = 20/k_F$, $W = 6/k_F$, $D_{\text{SC}} = 10/k_F$ and $D_{2\text{DEG}} = 4/k_F$.

A mismatch in the Fermi velocity of the electron in the superconductor and 2DEG increases the amplitude of the normal reflections while decreasing that of Andreev reflections. Since the superconductivity in the 2DEG is proximity-induced via Andreev reflection processes at the interface [65, 66], the mismatch in turn reduces the strength of the proximity-induced gap.

These physical effects are illustrated more directly in Fig. 4. As shown in the top panel for the case where $\mu_S = \mu_{2\text{DEG}}$, the Fermi momentum mismatch between the superconductors and 2DEG increases as the SOC strength increases in the 2DEG which in turns reduces the proximity gap. The effect of the SOC on the proximity gap is less pronounced for the case where $\mu_S \gg \mu_{2\text{DEG}}$. This is shown in the lower panel of Fig. 4. In summary, to avoid this mismatch it helps to choose the chemical potential of the superconductor to be much larger than that of the 2DEG.

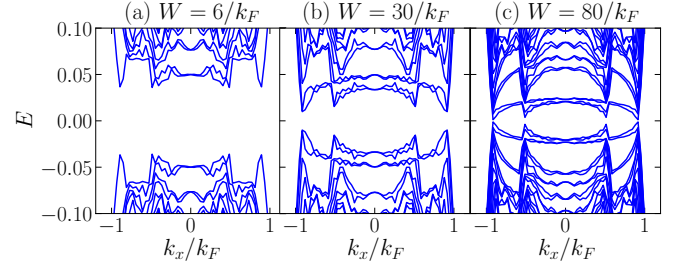


FIG. 5. Energy spectra of planar Josephson junctions for different junction widths: (a) $W = 6/k_F$, (b) $W = 30/k_F$, and (c) $W = 80/k_F$. The spectral gap decreases with increasing junction width W . The parameters used are: $\mu_{2\text{DEG}} = 1$, $\mu_S = 10$, $E_{Z,J} = E_{Z,L} = 0$, $\Delta_0 = 0.3$ [$\xi = v_F/(\pi\Delta_0) = 2.12/k_F$], $\phi = 0$, $W_{\text{SC}} = 20/k_F$, $D_{\text{SC}} = 10/k_F$ and $D_{2\text{DEG}} = 4/k_F$.

But this raises another important issue. While SOC effects suggest that a substantial mismatch in chemical potentials is favorable for proximitization, there is a negative side to making the chemical potential mismatch ($\delta\mu = \mu_S - \mu_{2\text{DEG}}$) too large. To make this clear, we can compare Fig. 4(a) and Fig. 4(d) which represent an extreme example of zero SOC in the 2DEG. Here one can see that the larger is the chemical potential difference the smaller the effective pairing gap. This is because the chemical potential mismatch increases the Fermi velocity mismatch between the 2DEG and the superconductors resulting in a decrease in the NS interface transparency. We will refer back to these competing effects involving $\delta\mu$ and the SOC strength, α , in a summary figure (Fig. 7) below, but we here emphasize the subtle tradeoffs which must be considered to optimize the outcome.

B. Effects of variable channel width and variable junction thickness

Figure 5 illustrates a striking effect of increasing the width of the quasi 1D channel of the junction in the 2DEG. The pairing gap is greatly suppressed as the channel becomes wider. This is relatively easy to understand, as proximitization strength (arising from the leaking of Cooper pairs from the superconductors to 2DEG) decays with increasing distance from the superconductors which results in a smaller superconducting gap for a wider junction between the two superconductors. We illustrate this case in part because this wide channel situation is more favorable for observing the FFLO phase discussed in Section VIII.

Figure 6 addresses the thickness of the 2DEG, illustrating another effect associated with geometry. Shown here are plots of the pair amplitude (upper panel) and energy spectra (lower panel) of the Josephson junction. It can be seen from the plots that the pair amplitude and spectral gap decrease with increasing thickness of the 2DEG. There are contrary suggestions in the liter-

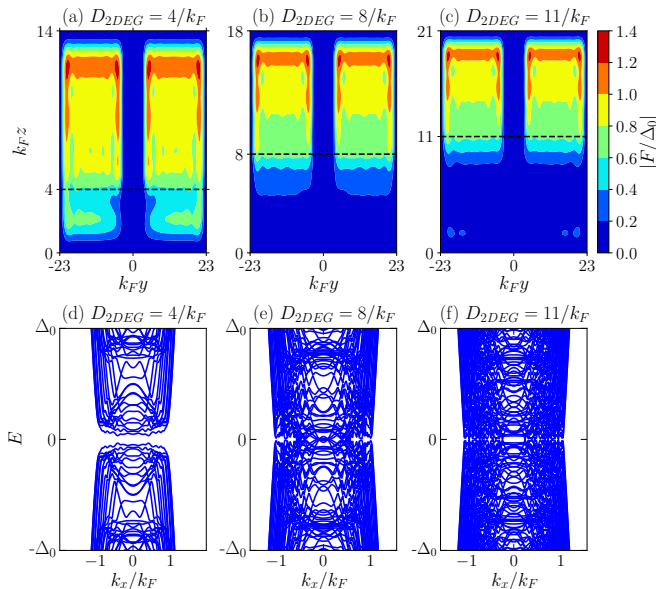


FIG. 6. Thickness effects. Profile of pair amplitude (Top panel) and energy spectra (Bottom panel) of planar Josephson junctions for zero Zeeman field and different thickness of 2DEG: $D_{2\text{DEG}} = 4/k_F$ (Left panel), $D_{2\text{DEG}} = 8/k_F$ (Middle panel) and $D_{2\text{DEG}} = 11/k_F$ (Right panel). Note that the thicker the 2DEG is, the smaller is the induced spectral gap in the 2DEG. The black dashed lines in the top panel denote the boundaries between the superconductors and the 2DEG. The parameters used are $\mu_S = 1$, $\mu_{2\text{DEG}} = 1$, $\alpha = 0.05$, $E_{Z,J} = E_{Z,L} = 0$, $\Delta_0 = 0.3$ [$\xi = v_F/(\pi\Delta_0) = 2.12/k_F$], $\phi = 0$, $W_{SC} = 20/k_F$, $W = 6/k_F$, $D_{SC} = 10/k_F$.

ature [64, 67] that these thicker substrates could be favorable as they allow “multi-channel participation.” As shown here, though, thicker junctions lead to smaller proximity gaps since they require that the superconducting correlations extend over a greater distance deeper into the 2DEG. We, thus, conclude that as Majorana zero modes are protected by large proximity-induced gaps, thinner 2DEGs are more favorable to be used as platforms for topological quantum computation.

Figure 7 presents a summary of how Δ^{prox} is affected by geometry and materials parameters. This figure shows how increasing (a) the thickness, (b) the chemical potential difference and (c) the SOC strength affect the proximity gap (at zero Zeeman field and zero phase difference). Clearly making both the thickness and the channel width larger has deleterious effects. However, as shown in Fig. 7(b) and Fig. 7(c), the effects of SOC are strongly connected to the magnitude of the chemical potential difference $\delta\mu$. When there is any finite SOC, there is a notable non-monotonicity in plots of Δ^{prox} versus $\delta\mu$. The initial rise in Δ^{prox} is due to the mismatch between the band structure of the superconductor with the Rashba-derived band structure in the 2DEG, as illustrated in Fig. 3. However, once the chemical potential difference is sufficiently large, as might be expected, increasing it further has a negative effect on the proximity gap. There

seems to be a “sweet spot” around $\delta\mu \approx 10$ which is substantially below the more realistic physical regime (where $\delta\mu$ might approach 100 or larger). Overall this figure should help guide materials parameters and geometries.

VI. SYMMETRY CLASS

It is useful to look at the underlying symmetries which dictate the nature of the topological phases. The above BdG Hamiltonian [Eq. (7)] for the planar Josephson junction commutes with the particle-hole symmetry operator $\mathcal{P} = \sigma_y \tau_y \mathcal{K}$ where \mathcal{K} is the complex conjugation. For zero Zeeman field $E_Z = 0$ and a superconducting phase bias $\phi = 0$ or $\phi = \pi$, the Hamiltonian belongs to the symmetry class DIII in the tenfold classification [68–70] as it also commutes with the time-reversal symmetry operator $\mathcal{T} = -i\sigma_y \mathcal{K}$ (where $\mathcal{T}^2 = -\mathbb{1}$). Moreover, the system also has a mirror symmetry along the x - z plane, i.e., $\mathcal{M}_y = -\sigma_y \times (y \rightarrow -y)$.

The \mathcal{T} and \mathcal{M}_y symmetries are broken when an in-plane Zeeman field is applied along the junction (x direction) or for a phase bias other than $\phi = 0$ or $\phi = \pi$. The Hamiltonian, however, remains invariant under an anti-unitary “effective” time-reversal operator $\tilde{\mathcal{T}}$ which is the product of the \mathcal{T} and \mathcal{M}_y operators, i.e., $\tilde{\mathcal{T}} = \mathcal{M}_y \mathcal{T} = i\mathcal{K} \times (y \rightarrow -y)$ where $\tilde{\mathcal{T}}^2 = \mathbb{1}$. Thus the system has the BDI symmetry [11, 12]. Moreover, since the Hamiltonian possesses $\tilde{\mathcal{T}}$ and \mathcal{P} symmetries, it also has a chiral symmetry, where the Hamiltonian anticommutes with the chirality operator $\mathcal{C} = -i\mathcal{P}\tilde{\mathcal{T}} = \mathcal{M}_y \tau_y$. When the $\tilde{\mathcal{T}}$ symmetry is broken, the symmetry class is reduced from class BDI to class D. In this case, an even number of Majorana zero modes at the same end of the junction couples to each other and splits into finite-energy mode leaving either zero or one Majorana mode at each end of the junction. This BDI symmetry can be broken by disorder [71], applying a transverse Zeeman field perpendicular to the junction (along y direction) [72] or having left and right superconductors with different widths or pairing potentials [11, 12, 72].

The symmetry class BDI is characterized by a \mathbb{Z} topological invariant Q_Z where $|Q_Z|$ denotes the number of Majorana zero modes at each end of the junctions. On the other hand, the symmetry class D is characterized by a \mathbb{Z}_2 topological invariant Q_{Z_2} which denotes the parity of the Q_Z invariant.

VII. TOPOLOGICAL PHASE DIAGRAM AND TRANSITION

The interest in nanowires associated with the Josephson junction architecture is, of course, related to the stability of topological phases. We obtain the phase diagram of the system by calculating the topological invariant following Ref. [73]. The numerical computation is consider-

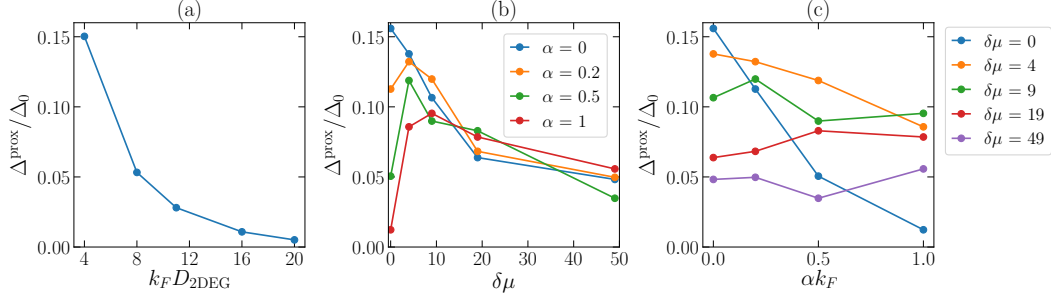


FIG. 7. Summary figure showing how Δ^{prox} depends on 2DEG thickness, $\delta\mu$ and SOC. (a) Induced gap $\Delta^{\text{prox}}/\Delta_0$ as a function of the 2DEG thickness $D_{2\text{DEG}}$ for SOC strength $\alpha = 0.05$ and $\mu_S = \mu_{2\text{DEG}} = 1$. The induced gap decreases with increasing 2DEG thickness. (b) Induced gap $\Delta^{\text{prox}}/\Delta_0$ as a function of chemical potential difference ($\delta\mu = \mu_S - \mu_{2\text{DEG}}$) calculated for $\mu_{2\text{DEG}} = 1$, $D_{2\text{DEG}} = 4/k_F$ and several values of SOC strength α . For small α , the induced gap decreases with increasing $\delta\mu$. For large α , the induced gap has nonmonotonic dependences on $\delta\mu$ where it first increases with increasing $\delta\mu$, rises to a maximum, and after reaching the maximum it decreases with increasing $\delta\mu$. (c) Induced gap $\Delta^{\text{prox}}/\Delta_0$ as a function of SOC strength α for $D_{2\text{DEG}} = 4/k_F$ and different values of $\delta\mu$. For small $\delta\mu$, the induced gap depends strongly on α where it decreases with increasing α . For the case where μ_S is much bigger than $\mu_{2\text{DEG}}$, the induced gap depends weakly on α . The parameters used for the above plots are $W_{\text{SC}} = 20/k_F$, $W = 6/k_F$, $D_{\text{SC}} = 10/k_F$, $E_{Z,J} = E_{Z,L} = 0$, $\Delta_0 = 0.3$, and $\mu_{2\text{DEG}} = 1$.

ably more complicated in the presence of our full treatment of proximitization. To do so, we first diagonalize the chiral operator \mathcal{C} with $\mathbb{1}$ and $-\mathbb{1}$ in the upper-left and lower-right block, respectively. Since $\{\mathcal{C}, \mathcal{H}\} = 0$, in this basis where the \mathcal{C} is block-diagonal, the BdG Hamiltonian \mathcal{H}_{k_x} is off-diagonal, i.e.,

$$UCU^\dagger = \begin{pmatrix} \mathbb{1} & 0 \\ 0 & -\mathbb{1} \end{pmatrix}, \quad (23a)$$

$$U\mathcal{H}_{k_x}U^\dagger = \begin{pmatrix} 0 & A(k_x) \\ A^\dagger(-k_x) & 0 \end{pmatrix}. \quad (23b)$$

We can calculate the \mathbb{Z} topological invariant ($Q_{\mathbb{Z}}$) from the winding of the phase $\theta(k_x)$ of the determinant of the off-diagonal part $A(k_x)$ where $e^{i\theta(k_x)} = \det A(k_x)/|\det A(k_x)|$. The \mathbb{Z} topological invariant is given by

$$Q_{\mathbb{Z}} = \int_0^\infty \frac{dk_x}{\pi} \frac{d\theta(k_x)}{dk_x}, \quad (24)$$

and the \mathbb{Z}_2 topological invariant (the parity of $Q_{\mathbb{Z}}$) is given by

$$Q_{\mathbb{Z}_2} = (-1)^{Q_{\mathbb{Z}}}. \quad (25)$$

It is shown in Ref. [73] that Eq. (25) is simply the \mathbb{Z}_2 Pfaffian invariant of 1D systems [74], i.e.,

$$Q_{\mathbb{Z}_2} = \text{sgn} \frac{\text{Pf}[(\mathcal{H}_{k_x \rightarrow \infty})\sigma_y\tau_y]}{\text{Pf}[(\mathcal{H}_{k_x=0})\sigma_y\tau_y]}. \quad (26)$$

Figures 8 and 9 present the phase diagrams of the planar Josephson junction obtained from the full proximity calculations. These phase diagrams emphasize the novel feature of the junction architecture which enables the topological phase to be tuned either by changing the phase bias or the Zeeman field.

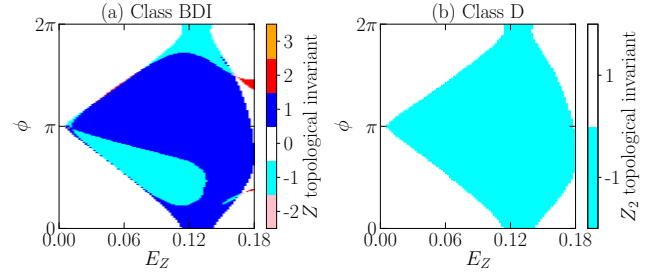


FIG. 8. Topological phase diagram for a proximitized Josephson junction with vanishing chemical potential mismatch $\delta\mu = 0$. (a) Class BDI and (b) Class D phase diagrams as functions of E_Z and ϕ . Each region is labeled by different \mathbb{Z} topological invariants in the BDI phase diagram. The \mathbb{Z}_2 invariant gives the parity of the \mathbb{Z} index. The topological invariant $Q_{\mathbb{Z}_2} = -1$ and $Q_{\mathbb{Z}_2} = 1$ corresponds to the odd and even \mathbb{Z} indices which in turn indicates the topological and trivial phases of class D. The parameters used are $\mu_S = \mu_{2\text{DEG}} = 1$, $\alpha = 0.05$, $\Delta_0 = 0.3$, $W_{\text{SC}} = 20/k_F$, $W = 6/k_F$, $D_{\text{SC}} = 10/k_F$ and $D_{2\text{DEG}} = 4/k_F$.

Figure 8 shows the class BDI and class D phase diagrams for the same junction. Each phase in the BDI phase diagram [Fig. 8(a)] is labeled by a different \mathbb{Z} topological invariant ($Q_{\mathbb{Z}}$) where $|Q_{\mathbb{Z}}|$ denotes the number of Majorana zero modes located at each end of the junction. As can be seen from Fig. 8(a), the $\mathbb{Z} = 1$ topological region occupies most of the phase diagram as it occurs in a wide range of parameters. The topological transition between each of the BDI phases is indicated by a gap closing at $k_x = k_F$. The class D phase diagram, on the other hand, [Fig. 8(b)] shows the parity of the \mathbb{Z} topological invariant [Eq. (25)] where $Q_{\mathbb{Z}_2} = 1$ and $Q_{\mathbb{Z}_2} = -1$ corresponds to the trivial and topological phases of class D, respectively. The topological transition between the

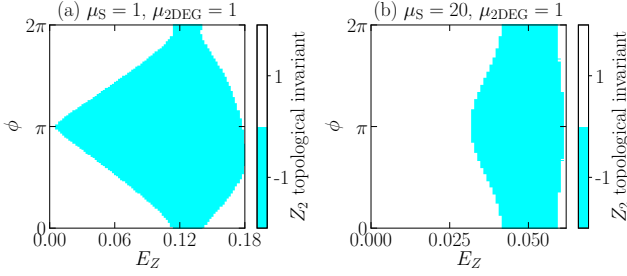


FIG. 9. Comparison of topological phase diagrams (a) without and (b) with chemical potential mismatch. Class D phase diagrams for two different values of chemical potential differences between the superconductors and the 2DEG: (a) $\mu_S = 1$ and $\mu_{2DEG} = 1$ and (b) $\mu_S = 20$ and $\mu_{2DEG} = 1$. The \mathbb{Z}_2 invariant $Q_{\mathbb{Z}_2} = -1$ and $Q_{\mathbb{Z}_2} = 1$ indicate the topological and trivial phases of class D. The chemical potential of the 2DEG is renormalized by the chemical potential of the superconductors resulting in a difference between the effective chemical potential of the 2DEG below the superconductor and that of the 2DEG in the junction. This difference increases as the mismatch between the superconductor and 2DEG chemical potential becomes larger which in turn increases the amplitude of normal reflections in the 2DEG. As a result, for larger chemical potential mismatch, the phase diagrams becomes more stripe-like (less dependent on ϕ) and the critical Zeeman field for $\phi = \pi$ shifts to a larger value. The parameters used are $\mu_{2DEG} = 1$, $\alpha = 0.05$, $\Delta_0 = 0.3$, $W_{SC} = 20/k_F$, $W = 6/k_F$, $D_{SC} = 10/k_F$ and $D_{2DEG} = 4/k_F$.

$Q_{\mathbb{Z}_2} = 1$ and $Q_{\mathbb{Z}_2} = -1$ regions is signified in a gap closing at $k_x = 0$ [74].

Figure 9 shows the effect of chemical potential mismatch ($\delta\mu = \mu_{SC} - \mu_{2DEG}$) on the phase dependence of the class D phase diagram. For ideal or “transparent” Josephson junctions, the phase diagram has a diamond shape where the critical Zeeman field at which the topological phase transition happens is considerably smaller for $\phi = \pi$ than for $\phi = 0$ [see Fig. 9(a)]. We observe that, with a larger value for $\delta\mu$, the phase diagram appears to be more stripe like as in Fig. 9(b). Here, the dependence of the phase diagram on the superconducting phase difference ϕ becomes weaker and the critical Zeeman field for $\phi = \pi$ shifts to a larger value [75].

We understand this stripe-like phase diagram as deriving from an increasing mismatch between the chemical potential of the superconductor and the 2DEG. This, in turn, should be viewed as leading to an increase in the strength of the normal reflections in the 2DEG. Due to the proximity to the superconductor, the chemical potential of the 2DEG directly in contact with the superconductor will be renormalized by that of the superconductor. As a result, there is a difference between the effective chemical potential of the 2DEG directly below the superconductor with the effective chemical potential of the 2DEG in the junction. This effectively creates a potential barrier for the electrons which in turn increases the strength of normal reflections.

We conclude this section by noting that under ideal circumstances (i.e., for transparent junctions with small $\delta\mu$), the critical Zeeman field needed to tune the system to topological phases can be greatly reduced for a phase bias $\phi = \pi$. One can infer from Fig. 9(b), that when $\delta\mu$ assumes a substantial (and physically reasonable) value, this gain in reduction of the critical Zeeman field by tuning the phase ϕ to be near π is mostly lost [76]. We note that similar to the effect of $\delta\mu$, decreasing the width of the superconducting leads also makes the phase diagram becomes less dependent on the phase bias due to the enhancement of multiple normal reflections at the interface between the superconductors and the vacuum [72].

A. Energy dispersion across the topological phase transition

The topological phase transition of class D is associated with a gap closing at $k_x = 0$ [74]. As can be seen from the phase diagram [Fig. 9(a)], the critical Zeeman field at which the transition happens is smaller when the superconducting phase difference ϕ is near π . To elucidate this phase diagram, we address the energy spectrum of the system as a function of k_x across the phase transition.

Figure 10 shows the evolution of the energy spectrum of a planar Josephson junction as the Zeeman field is tuned across the topological phase transition for two different values of superconducting phase differences: $\phi = 0$ (upper panel) and $\phi = \pi$ (lower panel). At a particular value of critical field E_Z , the gap at $k_x = 0$ closes [panels (b) and (e)] which reflects the transition between trivial and topological phases. The critical Zeeman field is reduced as $\phi \rightarrow \pi$.

We summarize this section by noting that despite the more indirect form of proximitization associated with this Josephson junction architecture, as compared with the nanowires of Fig. 1(b), we have presented strong evidence that proximitized topological phases exist. This topological superconductivity occurs even when there are no direct attractive interactions in the 2DEG channel. Nevertheless, in this Josephson junction configuration the proximity coupling guarantees that there is a finite pair amplitude within the channel.

VIII. PROXIMITY-INDUCED FFLO PHASE

An exotic superconducting state, characterized by non-zero center-of-mass momentum of Cooper pairs and spatially varying order parameter, may occur for certain materials in the presence of both magnetic field and superconductivity. Interestingly, the planar junctions discussed here are associated with this exotic form of superconductivity, referred to as the Fulde-Ferrell-Larkin-Ovchinnikov (FFLO) phase [41, 42]. Indeed, it is hard to find examples where this elusive phase, deriving from

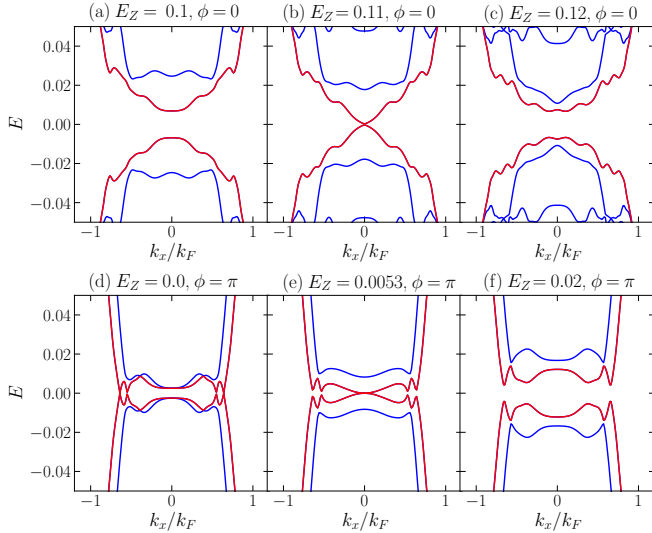


FIG. 10. Evolution of the energy spectrum of a planar Josephson junction across the topological phase transition for $\phi = 0$ (upper panel) and $\phi = \pi$ (lower panel). The topological transition is characterized by a gap closing at $k_x = 0$ where the critical field at which the topological transition occurs is the smallest at $\phi = \pi$. The critical field for $\phi = 0$ and $\phi = \pi$ are $E_Z = 0.11$ [panel (b)] and $E_Z = 0.0053$ [panel (e)], respectively. Energy spectra shown correspond to the phase diagram of Fig. 8. The gap closes and reopens at $k_x = 0$ as the Zeeman field E_Z is respectively tuned towards and away from the critical field. (a,d) The system is in the trivial phase, (b,e) the system undergoes a topological phase transition with a gap closing at $k_x = 0$, (c,f) the system is in the topological phase. Shown here are only few low-energy states close to zero energy where the energy levels closest to zero energy are shown by red lines. Here, we take the Zeeman field to be uniform ($E_{Z,J} = E_{Z,L} = E_Z$) in the 2DEG. The parameters used are $\mu_S = 1$, $\mu_{2\text{DEG}} = 1$, $\Delta_0 = 0.3$, $\alpha = 0.05$, $W_{\text{SC}} = 20/k_F$, $W = 6/k_F$, $D_{\text{SC}} = 10/k_F$ and $D_{2\text{DEG}} = 4/k_F$.

magnetic field effects, has been observed [44] which does *not* originate from proximity coupling. Experiments based on this Josephson junction architecture [43] report that the FFLO phase appears to be confined within the 1D channel of the junction. One might have expected it to be present in some form throughout the 2DEG since magnetic fields and proximity coupling are present outside the channel as well. There, however, the induced gaps are stronger due to the close proximity to the superconductor. The channel in the junction which is well away from the host superconductors has greatly weakened pair amplitude with superconducting phases which are freer to oscillate in response to an applied in-plane Zeeman field.

The upper panel of Fig. 11 presents a contour plot of the pair amplitude $F(\mathbf{r})$ throughout the junction. We point out that the junctions considered here are very wide. They correspond to the widest case shown in Fig. 5(c) where the proximity gap is extremely small. This weak proximity gap is not favorable to topological

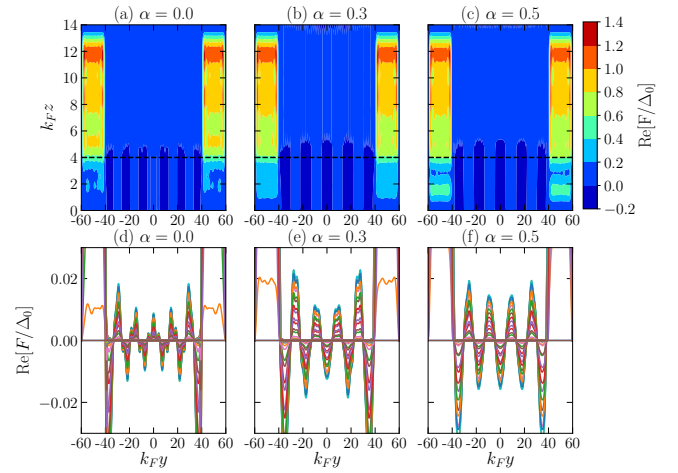


FIG. 11. Evidence for FFLO pairing. Profile of real part of the pair amplitude of planar Josephson junctions with 2D Rashba SOC of different strength: $\alpha = 0$ (Left panel), $\alpha = 0.3$ (Middle panel) and $\alpha = 0.5$ (Right panel). Upper panel shows the color plots of the pair amplitude $\text{Re}[F/\Delta_0]$, and the lower panel is the linecuts of the pair amplitude along the y direction at different values of z . As shown in the bottom panel, the pair amplitude oscillates along the y direction with a characteristic oscillation length $\lambda = E_Z/(2v_F)$ that decreases with increasing α since the Fermi velocity $v_F \propto \alpha$. The black dashed lines in the upper panel denote the boundary between the superconductors and the 2DEG. The parameters used are $\mu_S = 1$, $\mu_{2\text{DEG}} = 1$, $E_{Z,J} = E_{Z,L} = 0.3$, $\Delta_0 = 0.3$, $\phi = 0$, $W_{\text{SC}} = 20/k_F$, $W = 80/k_F$, $D_{\text{SC}} = 10/k_F$, $D_{2\text{DEG}} = 4/k_F$.

superconductivity. But, this figure should make it clear, however, that even though the channel is wide, the existence of a FFLO phase demonstrates that the channel should be viewed as a proximitized superconductor, rather than as a strictly “normal” region. Shown in three panels are the pair amplitudes for three different values of SOC strength. The lower panel presents linecuts of this pair amplitude along the y direction which show that, as in experiment [43], the oscillations of the pair amplitude are confined to the 2DEG channel. The frequency of these oscillations scales appropriately with both the applied Zeeman field and the SOC strength.

In Appendix A we show that the FFLO state also present for the case of 1D Rashba SOC. There we also illustrate how the same behavior can be found in the effective models where the superconducting hosts have been “integrated out”.

IX. CONCLUSIONS

While heterostructures that involve proximitization appear to be important for achieving topological superconductivity, the major components required to achieve this phase are in many ways inimical to the proximitization process. These involve Zeeman fields, spin-orbit coupling which can lead to band-structure mismatches and

substantial chemical potential discontinuities between the metallic host superconductors and the proximitized (often semiconducting) medium. Nevertheless, experiments [34, 35] seem to be demonstrating success. Although theoretically we might expect this proximitization to be a rather delicate and fragile process, nevertheless, we are able to show that there are clear indications of well-established topological superconductivity. The figures throughout this paper illustrate this situation. We stress that in our Josephson junction configuration the proximity is more remote compared to that in the conventional nanowire configuration of Fig. 1(b).

Because we have focused on the proximitization process itself, in this paper we were able to consider how to maximize the proximity gap Δ^{prox} both by varying geometry as well as materials parameters. This particular parameter is understood to be computed in the absence of Zeeman field or phase difference. It nevertheless sets the scale for the energy gap in the topological phase, E_{gap} , and, thereby for the stability of Majorana zero modes.

Figure 7 presents a summary of our major findings. One should aim for junctions with very thin 2DEG regions and narrow channels between the host superconductors. Additionally, there is a delicate competition between the chemical potential differences of the 2DEG and

the superconductors ($\delta\mu$), and the Rashba SOC strength. While a larger $\delta\mu$ serves to compensate for deleterious effects of SOC, it cannot be too big. Indeed, Fig. 9(b) shows that one major knob of the Josephson architecture (which is the ability to tune the phase difference to π and thereby require very small Zeeman fields to access topological phases) is undermined if $\delta\mu$ is too large.

Finally, by plotting the pair amplitude itself, we have provided in this paper very direct evidence for the elusive FFLO phase. It is not necessarily to be associated with topological physics, but it has some of the same requirements. We show how the presence of Zeeman fields together with SOC and (remote) proximity effect stabilize this state which exists entirely inside the 2DEG channel, much as in recent experiments [43].

ACKNOWLEDGMENTS

We thank Erez Berg for helpful conversations. This work was supported by NSF-DMR-MRSEC 1420709. C.-T.W. is supported by the MOST Grant No. 106-2112-M-009-001-MY2C. We acknowledge the University of Chicago Research Computing Center for support of this work.

-
- [1] Roman M. Lutchyn, Jay D. Sau, and S. Das Sarma, “Majorana fermions and a topological phase transition in semiconductor-superconductor heterostructures,” *Phys. Rev. Lett.* **105**, 077001 (2010).
 - [2] Yuval Oreg, Gil Refael, and Felix von Oppen, “Helical liquids and majorana bound states in quantum wires,” *Phys. Rev. Lett.* **105**, 177002 (2010).
 - [3] Jason Alicea, “New directions in the pursuit of majorana fermions in solid state systems,” *Reports on progress in physics* **75**, 076501 (2012).
 - [4] Martin Leijnse and Karsten Flensberg, “Introduction to topological superconductivity and majorana fermions,” *Semiconductor Science and Technology* **27**, 124003 (2012).
 - [5] Tudor D Stanescu and Sumanta Tewari, “Majorana fermions in semiconductor nanowires: fundamentals, modeling, and experiment,” *Journal of Physics: Condensed Matter* **25**, 233201 (2013).
 - [6] C W J Beenakker, “Search for majorana fermions in superconductors,” *Annu. Rev. Con. Mat. Phys.* **4**, 113–136 (2013).
 - [7] Steven R. Elliott and Marcel Franz, “Colloquium: Majorana fermions in nuclear, particle, and solid-state physics,” *Rev. Mod. Phys.* **87**, 137–163 (2015).
 - [8] Sankar Das Sarma, Michael Freedman, and Chetan Nayak, “Majorana zero modes and topological quantum computation,” *npj Quantum Information* **1**, 15001 (2015).
 - [9] Ramón Aguado, “Majorana quasiparticles in condensed matter,” *Riv. Nuovo Cimento* **40**, 523–593 (2018).
 - [10] RM Lutchyn, EPAM Bakkers, LP Kouwenhoven, P Krogstrup, CM Marcus, and Y Oreg, “Majorana zero modes in superconductor–semiconductor heterostructures,” *Nature Reviews Materials*, 1 (2018).
 - [11] Falko Pientka, Anna Keselman, Erez Berg, Amir Yacoby, Ady Stern, and Bertrand I. Halperin, “Topological superconductivity in a planar josephson junction,” *Phys. Rev. X* **7**, 021032 (2017).
 - [12] Michael Hell, Martin Leijnse, and Karsten Flensberg, “Two-dimensional platform for networks of majorana bound states,” *Phys. Rev. Lett.* **118**, 107701 (2017).
 - [13] V. Mourik, K. Zuo, S. M. Frolov, S. R. Plissard, E. P. A. M. Bakkers, and L. P. Kouwenhoven, “Signatures of majorana fermions in hybrid superconductor-semiconductor nanowire devices,” *Science* **336**, 1003–1007 (2012).
 - [14] Leonid P Rokhinson, Xinyu Liu, and Jacek K Furdyna, “The fractional ac josephson effect in a semiconductor-superconductor nanowire as a signature of majorana particles,” *Nat. Phys.* **8**, 795–799 (2012).
 - [15] M. T. Deng, C. L. Yu, G. Y. Huang, M. Larsson, P. Caroff, and H. Q. Xu, “Anomalous zero-bias conductance peak in a,” *Nano Lett.* **12**, 6414–6419 (2012).
 - [16] Anindya Das, Yuval Ronen, Yonatan Most, Yuval Oreg, Moty Heiblum, and Hadas Shtrikman, “Zero-bias peaks and splitting in an al-inas nanowire topological superconductor as a signature of majorana fermions,” *Nat. Phys.* **8**, 887–895 (2012).
 - [17] H. O. H. Churchill, V. Fatemi, K. Grove-Rasmussen, M. T. Deng, P. Caroff, H. Q. Xu, and C. M. Marcus, “Superconductor-nanowire devices from tunneling to the multichannel regime: Zero-bias oscillations and magnetoconductance crossover,” *Phys. Rev. B* **87**, 241401 (2013).

- [18] A. D. K. Finck, D. J. Van Harlingen, P. K. Mohseni, K. Jung, and X. Li, “Anomalous modulation of a zero-bias peak in a hybrid nanowire-superconductor device,” *Phys. Rev. Lett.* **110**, 126406 (2013).
- [19] Sven Marian Albrecht, AP Higginbotham, Morten Madsen, Ferdinand Kuemmeth, Thomas Sand Jespersen, Jesper Nygård, Peter Krogstrup, and CM Marcus, “Exponential protection of zero modes in majorana islands,” *Nature* **531**, 206 (2016).
- [20] Önder Gül, Hao Zhang, Jouri DS Bommer, Michiel WA de Moor, Diana Car, Sébastien R Plissard, Erik PAM Bakkers, Attila Geresdi, Kenji Watanabe, Takashi Taniguchi, *et al.*, “Ballistic majorana nanowire devices,” *Nature nanotechnology* **13**, 192 (2018).
- [21] Jun Chen, Peng Yu, John Stenger, Moira Hovevar, Diana Car, Sébastien R Plissard, Erik PAM Bakkers, Tudor D Stanescu, and Sergey M Frolov, “Experimental phase diagram of zero-bias conductance peaks in superconductor/semiconductor nanowire devices,” *Science advances* **3**, e1701476 (2017).
- [22] MT Deng, S Vaitiekėnas, Esben Bork Hansen, Jeroen Danon, M Leijnse, Karsten Flensberg, Jesper Nygård, P Krogstrup, and Charles M Marcus, “Majorana bound state in a coupled quantum-dot hybrid-nanowire system,” *Science* **354**, 1557–1562 (2016).
- [23] H. J. Suominen, M. Kjaergaard, A. R. Hamilton, J. Shabani, C. J. Palmström, C. M. Marcus, and F. Nichele, “Zero-energy modes from coalescing andreev states in a two-dimensional semiconductor-superconductor hybrid platform,” *Phys. Rev. Lett.* **119**, 176805 (2017).
- [24] Fabrizio Nichele, Asbjørn C. C. Drachmann, Alexander M. Whiticar, Eoin C. T. O’Farrell, Henri J. Suominen, Antonio Fornieri, Tian Wang, Geoffrey C. Gardner, Candice Thomas, Anthony T. Hatke, Peter Krogstrup, Michael J. Manfra, Karsten Flensberg, and Charles M. Marcus, “Scaling of majorana zero-bias conductance peaks,” *Phys. Rev. Lett.* **119**, 136803 (2017).
- [25] Hao Zhang, Chun-Xiao Liu, Sasa Gazibegovic, Di Xu, John A Logan, Guanzhong Wang, Nick Van Loo, Jouri DS Bommer, Michiel WA De Moor, Diana Car, *et al.*, “Quantized majorana conductance,” *Nature* **556**, 74 (2018).
- [26] Hao Zhang, Önder Gül, Sonia Conesa-Boj, Michał P Nowak, Michael Wimmer, Kun Zuo, Vincent Mourik, Folkert K De Vries, Jasper Van Veen, Michiel WA De Moor, *et al.*, “Ballistic superconductivity in semiconductor nanowires,” *Nature communications* **8**, 16025 (2017).
- [27] Joachim E. Sestoft, Thomas Kanne, Aske Nørskov Gejl, Merlin von Soosten, Jeremy S. Yodh, Daniel Sherman, Brian Tarasinski, Michael Wimmer, Erik Johnson, Mingtang Deng, Jesper Nygård, Thomas Sand Jespersen, Charles M. Marcus, and Peter Krogstrup, “Engineering hybrid epitaxial inasb/al nanowires for stronger topological protection,” *Phys. Rev. Materials* **2**, 044202 (2018).
- [28] M.-T. Deng, S. Vaitiekėnas, E. Prada, P. San-Jose, J. Nygård, P. Krogstrup, R. Aguado, and C. M. Marcus, “Nonlocality of majorana modes in hybrid nanowires,” *Phys. Rev. B* **98**, 085125 (2018).
- [29] Dominique Laroche, Daniël Bouman, David J van Woerkom, Alex Proutski, Chaitanya Murthy, Dmitry I Pikulin, Chetan Nayak, Ruben JJ van Gulik, Jesper Nygård, Peter Krogstrup, *et al.*, “Observation of the 4π -periodic josephson effect in inas nanowires,” *Nature Communications* **10**, 245 (2019).
- [30] Jasper van Veen, Alex Proutski, Torsten Karzig, Dmitry I. Pikulin, Roman M. Lutchyn, Jesper Nygård, Peter Krogstrup, Attila Geresdi, Leo P. Kouwenhoven, and John D. Watson, “Magnetic-field-dependent quasiparticle dynamics of nanowire single-cooper-pair transistors,” *Phys. Rev. B* **98**, 174502 (2018).
- [31] Michiel WA de Moor, Jouri DS Bommer, Di Xu, Georg W Winkler, Andrey E Antipov, Arno Bargerbos, Guanzhong Wang, Nick van Loo, Roy LM Veld, Sasa Gazibegovic, *et al.*, “Electric field tunable superconductor-semiconductor coupling in majorana nanowires,” *New Journal of Physics* **20**, 103049 (2018).
- [32] Anna Grivnin, Ella Bor, Moty Heiblum, Yuval Oreg, and Hadas Shtrikman, “Concomitant opening of a topological bulk-gap with an emerging majorana edge-state,” *arXiv preprint arXiv:1807.06632* (2018).
- [33] S Vaitiekėnas, M-T Deng, P Krogstrup, and CM Marcus, “Flux-induced majorana modes in full-shell nanowires,” *arXiv preprint arXiv:1809.05513* (2018).
- [34] Hechen Ren, Falko Pientka, Sean Hart, Andrew Pierce, Michael Kosowsky, Lukas Lunczer, Raimund Schlereth, Benedikt Scharf, Ewelina M. Hankiewicz, Laurens W. Molenkamp, Bertrand I. Halperin, and Amir Yacoby, “Topological superconductivity in a phase-controlled josephson junction,” *arXiv:1809.03076* (2018).
- [35] Antonio Fornieri, Alexander M. Whiticar, F. Setiawan, Elías Portolés Marín, Asbjørn C. C. Drachmann, Anna Keselman, Sergei Gronin, Candice Thomas, Tian Wang, Ray Kallaher, Geoffrey C. Gardner, Erez Berg, Michael J. Manfra, Ady Stern, Charles M. Marcus, and Fabrizio Nichele, “Evidence of topological superconductivity in planar josephson junctions,” *arXiv:1809.03037* (2018).
- [36] W. L. McMillan, “Tunneling model of the superconducting proximity effect,” *Phys. Rev.* **175**, 537–542 (1968).
- [37] W. L. McMillan, “Theory of superconductor—normal-metal interfaces,” *Phys. Rev.* **175**, 559–568 (1968).
- [38] Jay D. Sau, Roman M. Lutchyn, Sumanta Tewari, and S. Das Sarma, “Robustness of majorana fermions in proximity-induced superconductors,” *Phys. Rev. B* **82**, 094522 (2010).
- [39] Tudor D. Stanescu, Jay D. Sau, Roman M. Lutchyn, and S. Das Sarma, “Proximity effect at the superconductor—topological insulator interface,” *Phys. Rev. B* **81**, 241310 (2010).
- [40] Andrew C. Potter and Patrick A. Lee, “Engineering a $p+i$ superconductor: Comparison of topological insulator and rashba spin-orbit-coupled materials,” *Phys. Rev. B* **83**, 184520 (2011).
- [41] Peter Fulde and Richard A. Ferrell, “Superconductivity in a strong spin-exchange field,” *Phys. Rev.* **135**, A550 (1964).
- [42] AI Larkin and Yu N Ovchinnikov, “Nonuniform state of superconductors,” *Zh. Eksp. Teor. Fiz.* **47**, 1136 (1964).
- [43] Sean Hart, Hechen Ren, Michael Kosowsky, Gilad Ben-Shach, Philipp Leubner, Christoph Brüne, Hartmut Buhmann, Laurens W Molenkamp, Bertrand I Halperin, and Amir Yacoby, “Controlled finite momentum pairing and spatially varying order parameter in proximitized hgte quantum wells,” *Nature Physics* **13**, 87 (2017).

- [44] Angela Q Chen, Moon Jip Park, Stephen T Gill, Yiran Xiao, Dalmau Reig-i Plessis, Gregory J MacDougall, Matthew J Gilbert, and Nadya Mason, “Finite momentum cooper pairing in three-dimensional topological insulator josephson junctions,” *Nature communications* **9**, 3478 (2018).
- [45] Stevan Nadj-Perge, Ilya K Drozdov, Jian Li, Hua Chen, Sangjun Jeon, Jungpil Seo, Allan H MacDonald, B Andrei Bernevig, and Ali Yazdani, “Observation of majorana fermions in ferromagnetic atomic chains on a superconductor,” *Science* **346**, 602 (2014).
- [46] Jelena Klinovaja, Peter Stano, Ali Yazdani, and Daniel Loss, “Topological superconductivity and majorana fermions in rkky systems,” *Phys. Rev. Lett.* **111**, 186805 (2013).
- [47] S. Nadj-Perge, I. K. Drozdov, B. A. Bernevig, and Ali Yazdani, “Proposal for realizing majorana fermions in chains of magnetic atoms on a superconductor,” *Phys. Rev. B* **88**, 020407 (2013).
- [48] Jian Li, Hua Chen, Ilya K. Drozdov, A. Yazdani, B. Andrei Bernevig, and A. H. MacDonald, “Topological superconductivity induced by ferromagnetic metal chains,” *Phys. Rev. B* **90**, 235433 (2014).
- [49] J Li, T Neupert, Z Wang, A H MacDonald, Y Yazdani, and A Bernevig, “Two-dimensional chiral topological superconductivity in shiba lattices,” *Nature Communications* **7**, 12297 (2016).
- [50] P. M. R. Brydon, S. Das Sarma, Hoi-Yin Hui, and Jay D. Sau, “Topological yu-shiba-rusinov chain from spin-orbit coupling,” *Phys. Rev. B* **91**, 064505 (2015).
- [51] Hoi-Yin Hui, PMR Brydon, Jay D Sau, S Tewari, and S Das Sarma, “Majorana fermions in ferromagnetic chains on the surface of bulk spin-orbit coupled s-wave superconductors,” *Scientific reports* **5**, 8880 (2015).
- [52] Liang Fu and C. L. Kane, “Superconducting proximity effect and majorana fermions at the surface of a topological insulator,” *Phys. Rev. Lett.* **100**, 096407 (2008).
- [53] Jin-Peng Xu, Mei-Xiao Wang, Zhi Long Liu, Jian-Feng Ge, Xiaojun Yang, Canhua Liu, Zhu An Xu, Dandan Guan, Chun Lei Gao, Dong Qian, Ying Liu, Qiang-Hua Wang, Fu-Chun Zhang, Qi-Kun Xue, and Jin-Feng Jia, “Experimental detection of a majorana mode in the core of a magnetic vortex inside a topological insulator-superconductor $\text{Bi}_2\text{Te}_3/\text{NbSe}_2$ heterostructure,” *Phys. Rev. Lett.* **114**, 017001 (2015).
- [54] Hao-Hua Sun, Kai-Wen Zhang, Lun-Hui Hu, Chuang Li, Guan-Yong Wang, Hai-Yang Ma, Zhu-An Xu, Chun-Lei Gao, Dan-Dan Guan, Yao-Yi Li, Canhua Liu, Dong Qian, Yi Zhou, Liang Fu, Shao-Chun Li, Fu-Chun Zhang, and Jin-Feng Jia, “Majorana zero mode detected with spin selective andreev reflection in the vortex of a topological superconductor,” *Phys. Rev. Lett.* **116**, 257003 (2016).
- [55] Jay D. Sau, B. I. Halperin, K. Flensberg, and S. Das Sarma, “Number conserving theory for topologically protected degeneracy in one-dimensional fermions,” *Phys. Rev. B* **84**, 144509 (2011).
- [56] Ching-Kai Chiu, William S. Cole, and S. Das Sarma, “Induced spectral gap and pairing correlations from superconducting proximity effect,” *Phys. Rev. B* **94**, 125304 (2016).
- [57] Tudor D. Stanescu and S. Das Sarma, “Superconducting proximity effect in semiconductor nanowires,” *Phys. Rev. B* **87**, 180504 (2013).
- [58] Doru Sticlet, Bas Nijholt, and Anton Akhmerov, “Robustness of majorana bound states in the short-junction limit,” *Phys. Rev. B* **95**, 115421 (2017).
- [59] Tudor D. Stanescu and Sankar Das Sarma, “Proximity-induced low-energy renormalization in hybrid semiconductor-superconductor majorana structures,” *Phys. Rev. B* **96**, 014510 (2017).
- [60] Klaus Halterman and Oriol T. Valls, “Proximity effects at ferromagnet-superconductor interfaces,” *Phys. Rev. B* **65**, 014509 (2001).
- [61] Chien-Te Wu, Oriol T. Valls, and Klaus Halterman, “Proximity effects in conical-ferromagnet/superconductor bilayers,” *Phys. Rev. B* **86**, 184517 (2012).
- [62] Chien-Te Wu, Brandon M. Anderson, Wei-Han Hsiao, and K. Levin, “Majorana zero modes in spintronics devices,” *Phys. Rev. B* **95**, 014519 (2017).
- [63] Chien-Te Wu, F. Setiawan, Brandon M. Anderson, Wei-Han Hsiao, and K. Levin, “Quantum phase transitions in proximitized josephson junctions,” *Phys. Rev. B* **98**, 064504 (2018).
- [64] Tudor D. Stanescu, Roman M. Lutchyn, and S. Das Sarma, “Majorana fermions in semiconductor nanowires,” *Phys. Rev. B* **84**, 144522 (2011).
- [65] B Pannetier and H Courtois, “Andreev reflection and proximity effect,” *Journal of low temperature physics* **118**, 599–615 (2000).
- [66] TM Klapwijk, “Proximity effect from an andreev perspective,” *Journal of superconductivity* **17**, 593–611 (2004).
- [67] Roman M. Lutchyn, Tudor D. Stanescu, and S. Das Sarma, “Search for majorana fermions in multiband semiconducting nanowires,” *Phys. Rev. Lett.* **106**, 127001 (2011).
- [68] Alexei Kitaev, “Periodic table for topological insulators and superconductors,” in *AIP Conference Proceedings*, Vol. 1134 (AIP, 2009) pp. 22–30.
- [69] Shinsei Ryu, Andreas P Schnyder, Akira Furusaki, and Andreas WW Ludwig, “Topological insulators and superconductors: tenfold way and dimensional hierarchy,” *New Journal of Physics* **12**, 065010 (2010).
- [70] Alexander Altland and Martin R. Zirnbauer, “Non-standard symmetry classes in mesoscopic normal-superconducting hybrid structures,” *Phys. Rev. B* **55**, 1142–1161 (1997).
- [71] Arbel Haim and Ady Stern, “The double-edge sword of disorder in multichannel topological superconductors,” *arXiv e-prints*, arXiv:1808.07886 (2018), arXiv:1808.07886 [cond-mat.mes-hall].
- [72] F. Setiawan, Ady Stern, and Erez Berg, “Topological superconductivity in planar josephson junctions – narrowing down to the nanowire limit,” arXiv:1902.11300 (2019).
- [73] Sumanta Tewari and Jay D. Sau, “Topological invariants for spin-orbit coupled superconductor nanowires,” *Phys. Rev. Lett.* **109**, 150408 (2012).
- [74] A Yu Kitaev, “Unpaired majorana fermions in quantum wires,” *Physics-Uspekhi* **44**, 131 (2001).
- [75] The transparency of the interface between the superconductor and 2DEG is determined by the matching of the Fermi velocity between the two materials. While the difference between the Fermi energy of the superconductor and semiconductor can be of several orders of magnitude, the Fermi velocity between the two has a smaller

mismatch in magnitude because of a smaller electron effective mass of the semiconductor, which is not accommodated here. We note that the transparency is also affected by microscopic parameters such as the tunnel coupling strength and charge accumulation at the 2DEG-SC interface which are not accounted in our model.

[76] It can be noted that we use the same effective electron mass in the superconductor and 2DEG in addressing proximitization within this paper, and, thus, we may be overestimating the reduction in the phase dependence of the class D phase diagram and the proximity-induced gap due to the chemical potential mismatch $\delta\mu$.

- [77] Zhen Zheng, Ming Gong, Xubo Zou, Chuanwei Zhang, and Guangcan Guo, "Route to observable fulde-ferrell-larkin-ovchinnikov phases in three-dimensional spin-orbit-coupled degenerate fermi gases," *Phys. Rev. A* **87**, 031602 (2013).
- [78] Zhen Zheng, Ming Gong, Yichao Zhang, Xubo Zou, Chuanwei Zhang, and Guangcan Guo, "Fflo superfluids in 2d spin-orbit coupled fermi gases," *Scientific reports* **4**, 6535 (2014).
- [79] Da Wang, Zhoushen Huang, and Congjun Wu, "Fate and remnants of majorana zero modes in a quantum wire array," *Phys. Rev. B* **89**, 174510 (2014).

Appendix A: FFLO phases

We begin by studying the mechanism for the formation of the FFLO phases. In the absence of SOC, the Fermi surfaces of up and down-spins always form concentric circles as shown in Fig. A.1(a). For zero Zeeman fields, the superconducting pairing occurs between electrons carrying opposite spin with opposite momentum ($\mathbf{k} \uparrow$ and $-\mathbf{k} \downarrow$) on the Fermi surface where the Cooper pair has a zero center of mass momentum. If an in-plane magnetic field is applied to a system with no SOC, the Zeeman field enlarges and shrinks the Fermi surfaces radially in momentum by E_Z/v_F for the up and down spins, respectively, while keeping the two Fermi surfaces concentric. The pairing now occurs between the up- and down-spin electrons with different Fermi momenta, i.e., $\mathbf{k} + \mathbf{q}/2$ and $-\mathbf{k} + \mathbf{q}/2$ where $q = 2E_Z/v_F$, so that the Cooper pairs have a net center of mass momentum of \mathbf{q} . When the applied in-plane Zeeman field is sufficiently strong, spatial symmetry needs to be broken in order to lower the ground state energy which results in the FFLO state. However, because of the Pauli depairing, this FFLO state only survives in a narrow parameter regime. This depairing effect in strong Zeeman fields can be mitigated by using the SOC, which allows both singlet and triplet pairings, since the triplet pairing is not sensitive to the depairing effect.

In the presence of Rashba SOC, the Hamiltonian of a 2DEG without a Zeeman field [Eq. (7)] is invariant when the spin and momentum are rotated simultaneously in the x - y plane, i.e.,

$$\begin{pmatrix} -k'_y \\ k'_x \end{pmatrix} = \mathcal{R} \begin{pmatrix} -k_y \\ k_x \end{pmatrix}, \quad \begin{pmatrix} \sigma'_x \\ \sigma'_y \end{pmatrix} = \mathcal{R} \begin{pmatrix} \sigma_x \\ \sigma_y \end{pmatrix}, \quad (\text{A.1})$$

where

$$\mathcal{R} = \begin{pmatrix} \cos \theta & \sin \theta \\ -\sin \theta & \cos \theta \end{pmatrix} \quad (\text{A.2})$$

is the rotation operator in the x - y plane.

Note that the Hamiltonian still respects this rotational symmetry even in the presence of an out-of-plane Zeeman field (along z direction). However, the application of an in-plane Zeeman field E_Z along the junction i.e., along the x direction, breaks this rotational symmetry. The energy spectrum of the electron in the presence of the in-plane Zeeman field E_Z is given by

$$E = k_x^2 + k_y^2 - \mu + \frac{\alpha^2}{4} \pm \sqrt{\alpha^2 k_x^2 + (E_Z - \alpha k_y)^2}. \quad (\text{A.3})$$

which breaks the rotational symmetry.

In the limit where $E_Z \ll \alpha k_F \ll \mu$, the two Fermi surfaces are shifted in the direction perpendicular to the Zeeman field direction (along k_y) by $q = 2E_Z/v_F$ as shown in Fig. A.1(b). The pairing in this case occurs between up and down spins belonging to the same Fermi surface resulting also in Cooper pairs having a net momentum of \mathbf{q} . Thus the wave function of the Cooper pair can be written as $\cos(qy)|S\rangle + \sin(qy)|T\rangle$, where $|S\rangle = |\uparrow\downarrow\rangle - |\downarrow\uparrow\rangle$ and $|T\rangle = |\uparrow\downarrow\rangle + |\downarrow\uparrow\rangle$ are the singlet and triplet pairing wave functions, respectively. So, the presence of SOC stabilizes the FFLO phase as the SOC lifts the spin-degeneracy and shifts the Fermi surface in such a way that the resulting Cooper pair has a finite center of momentum [77, 78].

In the main text we have shown how the FFLO phase appears in a proximitized junction in the presence of an in-plane Zeeman field and a conventional (2D) Rashba SOC. In this appendix we show that our findings are quite robust, appearing also for a 1D Rashba SOC as well as in the effective model. We self-consistently solve the BdG

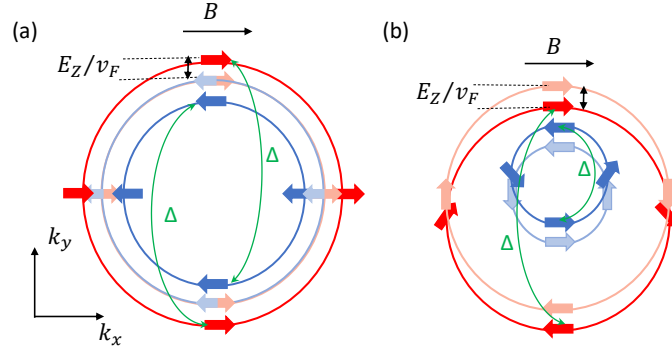


FIG. A.1. The change of Fermi surfaces of a 2DEG due to an in-plane magnetic field B along the junction (x direction) for the case of (a) zero SOC and (b) finite SOC strength. The Fermi surfaces in the absence and presence of B are represented by light and dark colors, respectively. (a) In the absence of a Zeeman field, the Fermi surfaces of a 2DEG without SOC are doubly degenerate. When an in-plane Zeeman field is applied, the Fermi surfaces of the up- and down-spins enlarge and shrink radially in momentum by E_Z/v_F while keeping the two Fermi surfaces concentric. The superconducting term Δ pairs up electrons with opposite spin from different Fermi surfaces. (b) The 2D Rashba SOC causes a clockwise and anticlockwise spin orientation (represented by red and blue arrows, respectively). The applied in-plane Zeeman field along x -direction shifts the inner and outer Fermi surfaces in the opposite direction along k_y by E_Z/v_F . The superconductivity term Δ pairs up electrons with opposite spin from the same Fermi surface.

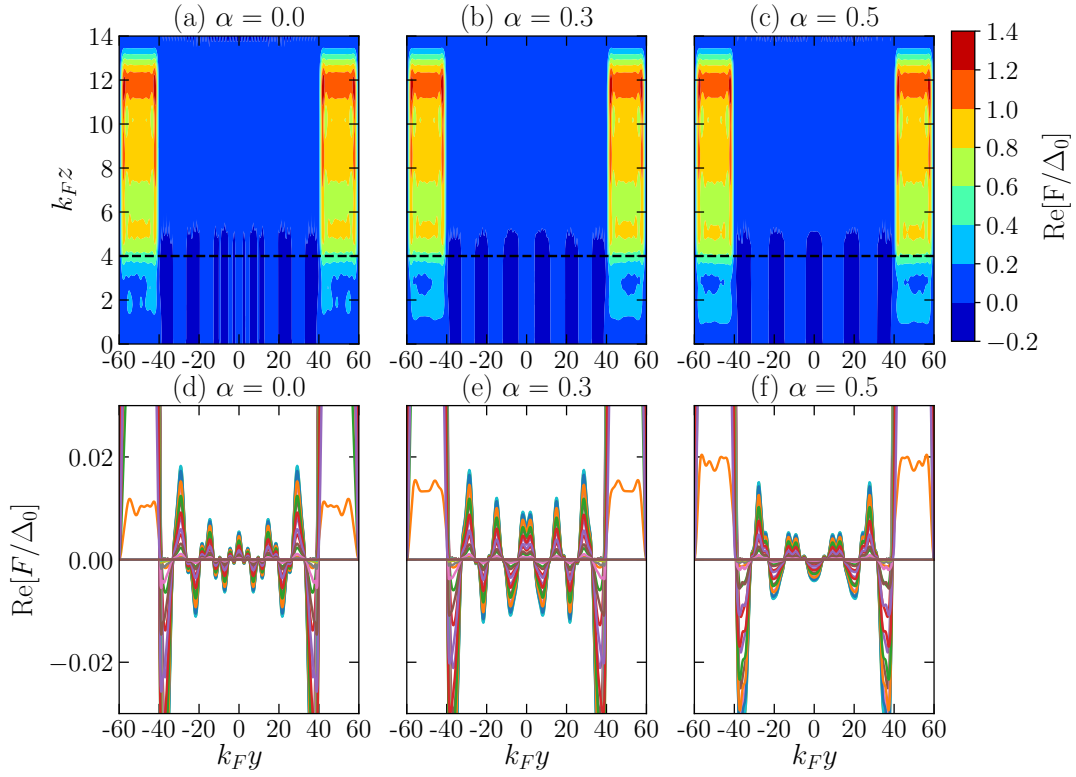


FIG. A.2. Evidence for FFLO. Profile of real part of the pair amplitude of a planar Josephson junction with a 1D Rashba SOC ($\alpha\partial_y\sigma_x$) of different strengths: $\alpha = 0$ (Left panel), $\alpha = 0.3$ (Middle panel) and $\alpha = 0.5$ (Right panel). Upper panel shows the color plots of the pair amplitude $\text{Re}[F_0/\Delta_0]$ and lower panel shows the linecuts of the pair amplitude along the y direction at different values of z . As shown in the lower panel, the pair amplitude oscillates along the y -direction with a characteristic oscillation length $\lambda = E_Z/(2v_F)$ that decreases with increasing α since $v_F \propto \alpha$. The black dashed lines in the upper panel denote the boundaries between the superconductors and the 2DEG. The parameters used are $\mu_S = 1$, $\mu_{2\text{DEG}} = 1$, $E_{Z,J} = E_{Z,L} = 0.2$, $\Delta_0 = 0.3$, $\phi = 0$, $W_{\text{SC}} = 20/k_F$, $W = 80/k_F$, $D_{\text{SC}} = 10/k_F$, $D_{2\text{DEG}} = 4/k_F$.

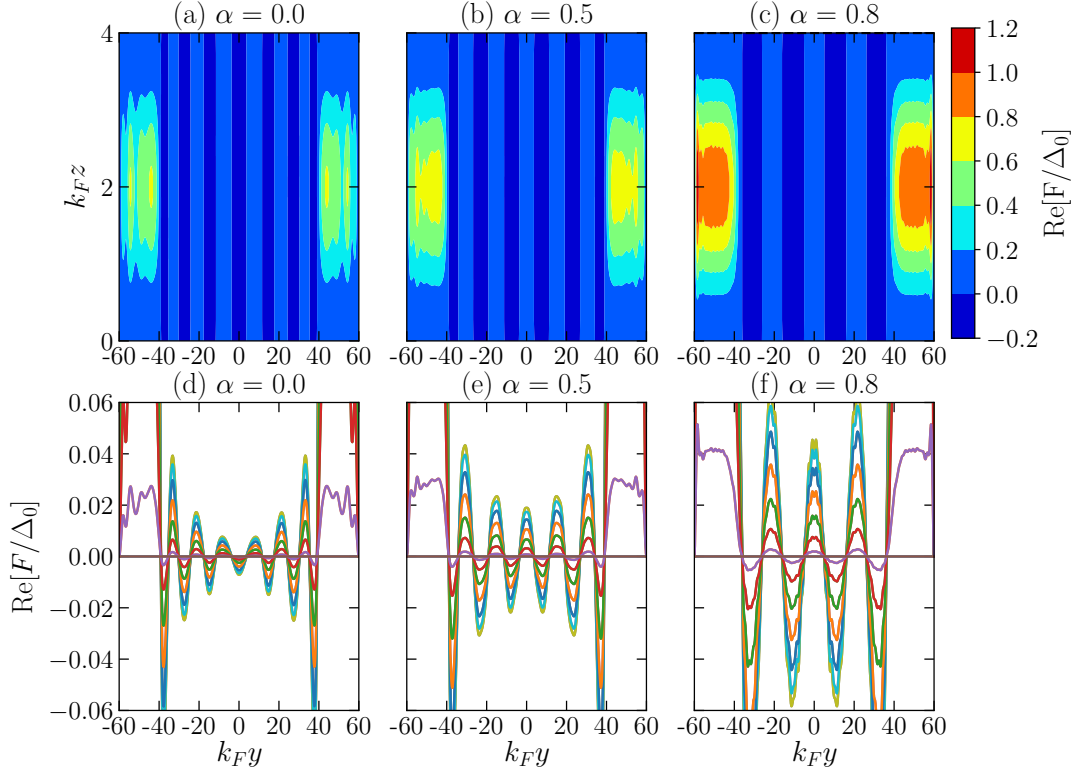


FIG. A.3. Evidence for FFLO. Profile of real part of the pair amplitude for the effective model of a planar Josephson junction[Eq. (21) of the main text]. The pair amplitudes are calculated for a 2D Rashba SOC of different strengths: $\alpha = 0$ (Left panel), $\alpha = 0.5$ (Middle panel) and $\alpha = 0.8$ (Right panel). Upper panel shows the color plots of the pair amplitude $\text{Re}[F_0/\Delta_0]$, and lower panel shows the linecuts of the pair amplitude along the y direction at different values of z . As shown in the lower panel, the pair amplitude oscillates along the y -direction with a characteristic oscillation length $\lambda = E_Z/(2v_F)$ that decreases with increasing α since $v_F \propto \alpha$. The parameters used are $\mu_S = 1$, $\mu_{2\text{DEG}} = 1$, $E_{Z,J} = E_{Z,L} = 0.3$, $\Delta_0 = 0.3$, $\phi = 0$, $W_{\text{SC}} = 20/k_F$, $W = 80/k_F$, $D_{2\text{DEG}} = 4/k_F$.

equations to obtain the pair amplitude [as given by Eq. (10) of the main text]:

$$F(y, z) = \int dk_x \sum_{E_n < \omega_D} [u_{nk_x \uparrow} v_{nk_x \downarrow}^* - u_{nk_x \downarrow} v_{nk_x \uparrow}^*] \tanh\left(\frac{E_n}{2T}\right). \quad (\text{A.4})$$

Figure A.2 shows the pair amplitude $F(y, z)$ for a 2DEG with a 1D Rashba spin-orbit-coupling $\alpha \partial_y \sigma_x$. The pair amplitudes are calculated for different SOC strengths. As for the case of 2D Rashba spin-orbit-coupled electron gas, here we can also observe an oscillation of the pair amplitude within the junction channel and with the oscillation length scale given by $\lambda = E_Z/(2v_F)$ which increases with increasing Zeeman field E_Z and decreases with increasing Fermi velocity v_F where $v_F \propto \alpha$. This is indicative of the FFLO phases formed in the presence of an applied magnetic field along the junction. We note that the Hamiltonian of a 2DEG with a 1D Rashba SOC can be mapped by a gauge transformation into the Hamiltonian of a conical Holmium magnet (Ref. [63]) or coupled nanowires (Ref. [79]) which are also platforms for topological superconductor.

Finally, Fig. A.3 shows the pair amplitude $F(y, z)$ for the effective model [Eq. (21)] of a planar Josephson junction with a 2D Rashba SOC. As shown in the figure, in the presence of an in-plane magnetic field, the pair amplitude $F(\mathbf{r})$ oscillates inside the junction channel with an oscillation length which decreases with increasing SOC strength. Again, the oscillation is consistent with the formation of an FFLO phase in the presence of an in-plane magnetic field.